A silicon isotopic perspective on the contribution of diagenesis to the sedimentary silicon budget in the Southern Ocean

Ivia Closset, Mark A. Brzezinski, Damien Cardinal, Arnaud Dapoigny, Janice L. Jones, Rebecca S. Robinson

Available online at www.sciencedirect.com

ScienceDirect

Geochimica et Cosmochimica Acta 327 (2022) 298–313

Geochimica et Cosmochimica Acta

www.elsevier.com/locate/gca

A silicon isotopic perspective on the contribution of diagenesis to the sedimentary silicon budget in the Southern Ocean

Ivia Closset [a,*], Mark A. Brzezinski [a,b], Damien Cardinal [c], Arnaud Dapoigny [d], Janice L. Jones [a], Rebecca S. Robinson [d,e]

[a] Marine Science Institute, University of California Santa Barbara, Santa Barbara, CA, USA
[b] Department of Ecology Evolution and Marine Biology, University of California, Santa Barbara, CA, USA
[c] LOCEAN UMR 7159 Sorbonne Université/CNRS/IRD/MNHN, 4 place Jussieu – boite 100, F-75252 Paris, France
[d] Laboratoire des Sciences du Climat et de l'Environnement, CNRS, 91190 Gif-sur-Yvette, France
[e] Graduate School of Oceanography, University of Rhode Island, Narragansett, RI 02882, USA

Received 24 July 2021; accepted in revised form 12 April 2022; Available online 22 April 2022

Abstract

Diatoms are known to fractionate silicon isotopes during the formation of their frustules causing the silicon isotopic composition of biogenic silica to track the degree of silicic acid consumption in surface waters. Despite a growing body of work that uses this proxy to reconstruct past changes in silicic acid utilization, the understanding of the benthic silicon cycle, particularly the identification and quantification of the processes that potentially alter the silicon isotopic composition of biogenic silica during early diagenesis is still lacking. We investigated these processes by comparing the silicon isotopic composition of pore water silicic acid, biogenic silica and, for the first time, lithogenic silica from five sediment cores collected in the deep basin of the Southern Ocean representing a diversity of sedimentation regimes. Silicic acid concentrations and the isotopic composition of Southern Ocean pore waters were the result of a dynamic balance between the dissolution of biogenic silica, reactive lithogenic silica phases and Si re-precipitation with the relative importance of each processes differing significantly between regions. The results are consistent with the formation of authigenic alumino-silicates derived from dissolved biogenic silica in the Sub-Antarctic Zone and in the Antarctic Zone (on average 12 ± 5% and 17 ± 13%, respectively). Since this latter process can fractionate silicon isotopes, this implies that, even if the silicon isotopic composition of diatoms preserved in the sediments is a reliable proxy for silicic acid utilization in the past ocean, care must be taken to extract a clean biogenic silica phase free of authigenic clays and lithogenic phases from sediments to eliminate this potential bias when interpreting isotopic records.

Keywords: Silicon cycle; Silicon stable isotopes; Benthic nutrient fluxes; Early diagenesis; Southern Ocean

1. INTRODUCTION

The global biogeochemical cycle of silicon (Si) has received widespread attention because it is coupled with the marine carbon cycle which plays a crucial role in the regulation of global climate. In the water column, biogenic silica (hereafter referred to as $bSiO_2$) production is mainly dominated by photosynthetic diatoms, creating a mechanistic link between the transfer of $bSiO_2$ and organic matter

* Corresponding author.
E-mail addresses: ivia@ucsb.edu (I. Closset), markbrzezinski@ucsb.edu (M.A. Brzezinski), damien.cardinal@locean.ipsl.fr (D. Cardinal), arnaud.dapoigny@lsce.ipsl.fr (A. Dapoigny), ja_jones@ucsb.edu (Janice L. Jones), rebecca_r@uri.edu (R.S. Robinson).

https://doi.org/10.1016/j.gca.2022.04.010
0016-7037/

from its creation in well-lit surface waters to the sediments. Net $bSiO_2$ burial is the process through which Si is removed from the global ocean and is thus key to understanding whether the marine Si cycle is at steady state (Tréguer and De La Rocha, 2013). Biogenic silica burial was estimated by Tréguer and De La Rocha (2013) to be 6.3 ± 3.6 Tmol Si yr^{-1} and recently revised to 9.2 ± 1.6 Tmol Si yr^{-1} (Tréguer et al., 2021). This represents 59% of the total Si output for the global ocean, but only approximately 4% of the total $bSiO_2$ production in the surface ocean. This very low $bSiO_2$ burial efficiency results from the recycling of most Si through $bSiO_2$ dissolution in the surface ocean (more than 50% of the surface $bSiO_2$ production) and at the seawater-sediment interface (approximately 30% of the surface $bSiO_2$ production). The latter two processes play a crucial role in the Si biogeochemical cycle since they contribute to the deep dissolved Si pool that eventually returns to the surface ocean through upwelling and vertical mixing.

A major highlight of the recent revision of the Si marine biogeochemical cycle by Tréguer et al. (2021) is the re-evaluation of the contribution of sedimentary processes in the oceanic Si sink, such as early silica diagenesis or precipitation of siliceous minerals, from 13% (Tréguer and De la Rocha, 2013) to 30% of the global output flux. The high uncertainty associated with this estimate (4.7 ± 2.3 Tmol Si yr^{-1}) reveal our lack of understanding of the processes altering the benthic Si biogeochemical cycle and invite further investigations of the dynamics of Si cycling within the sediments.

The Southern Ocean plays a dominant role in the global marine Si cycle. About 30% of global silica production occurs in the Southern Ocean and it is the single largest global sink for sedimentary $bSiO_2$, removing nearly 2 Tmol Si y^{-1} (Tréguer, 2014). The Southern Ocean is the only ocean region where there is direct communication between the deep meridional ocean circulation and surface water processes with profound implications for Southern Ocean control of the distribution of silicic acid and of Si isotopes throughout the global ocean (e.g. de Souza et al., 2012a; Brzezinski and Jones, 2015; Holzer and Brzezinski, 2015). The importance of the Southern Ocean to the Si cycle has inspired investigations of how silicic acid utilization in this region have varied across the ice age cycles of Earth's recent history, often in the context of explaining the low pCO_2 levels during the glacial periods (e.g. Brzezinski et al., 2002; Beucher et al., 2007; Dumont et al., 2020). Silicon isotopes have proven to be a powerful tool for understanding Si cycling on unprecedented spatial and temporal scales both in the modern and past ocean. Substantial advances have occurred in our understanding of the evolution of the marine Si cycle through the use of the fossil record combined with isotope geochemistry (e.g. De La Rocha et al., 1998; Brzezinski et al., 2002; Conley et al., 2017). Paleoreconstructions of Si dynamics and their implications for climate that use the Si isotope proxy require a better understanding of the biogeochemical and isotopic behavior of this element, including during early diagenesis in the sediment. To date, only few studies have investigated processes affecting the Si isotope dynamics in marine sediments and pore waters, and these are almost exclusively from shallow continental shelves (Ehlert et al., 2016; Geilert et al., 2020; Ng et al., 2020; Cassarino et al., 2020). The present work compliments these efforts by providing the first examinations of Si isotope dynamics in deep ocean sediments along gradients in surface primary production and deep ocean sedimentation regimes.

The silicon isotopic composition ($\delta^{30}Si$) of a sample is expressed as a deviation (in parts per thousand, i.e. ‰) from the ratio of $^{30}Si/^{28}Si$ of the sample from the international reference standard NBS28 and can be calculated according to the following formula:

$$\delta^{30}Si = \left(\frac{R_{sample}}{R_{standard}} - 1\right) \times 1000 \quad (1)$$

Where R is the ratio of $^{30}Si/^{28}Si$ in the sample and standard. The Si isotopic composition of any silicon pool is set by the $\delta^{30}Si$ of the Si source and any transformations within or between Si pools that induce isotopic fractionation. Silicon is fractionated because chemical and biological reactions favor either ^{28}Si or ^{30}Si. The degree to which Si isotopes fractionate during a specific process varies, allowing isotope values to be used to diagnose and trace Si cycling in the modern and past ocean.

In the surface ocean, siliceous organisms (mostly diatoms) fractionate Si isotope during the formation of opal by preferentially assimilating the lighter ^{28}Si isotope, therefore leaving the seawater slightly enriched in the heavier isotopes (De La Rocha et al., 1997). As proportionally more silicic acid is consumed, the $\delta^{30}Si$ of both silicic acid and $bSiO_2$ increases simultaneously. The instantaneous isotope effect ($^{30}\varepsilon_{Si}$), which describes the isotopic fractionation of ^{28}Si and ^{30}Si between silicic acid and $bSiO_2$ during the formation of diatom frustules has been evaluated by various laboratory studies. In the marine environment, De La Rocha et al. (1997) estimated a $^{30}\varepsilon_{Si}$ value of −1.1‰ independent of temperature, growth rate, or diatom species for the three different diatoms tested. In addition, Milligan et al. (2004) showed that $^{30}\varepsilon_{Si}$ is independent of the ambient pCO_2 level which support a broader use of the $\delta^{30}Si$ proxy under various environmental conditions. However, a more recent study in laboratory-controlled conditions revealed some species dependency of $^{30}\varepsilon_{Si}$ (ranging from −0.54 to −2.09‰; Sutton et al., 2013) during diatom opal formation, and pointed out the relevance of diatom taxonomic analysis when using $\delta^{30}Si$ for reconstruction of Si utilization.

The global ocean is undersaturated with respect to $bSiO_2$ such that diatom frustules will dissolve if not protected by the organic layer covering the living cells (Bidle & Azam, 1999). Demarest et al. (2009) collected diatoms from the surface ocean, subjected them to dissolution in seawater and found that dissolution favored the loss of light isotopes from the solid with an associated isotope effect, $^{30}\varepsilon_{Diss}$, of −0.55‰. The magnitude of isotopic fractionation during $bSiO_2$ dissolution opposes that occurring during Si uptake by preferentially removing lighter isotopes from $bSiO_2$ and returning them to the dissolved pool (Sun et al., 2014). However, the role of isotopic fractionation associated with $bSiO_2$ dissolution in the sea is equivocal as frustules recovered from sediment cores, as opposed to

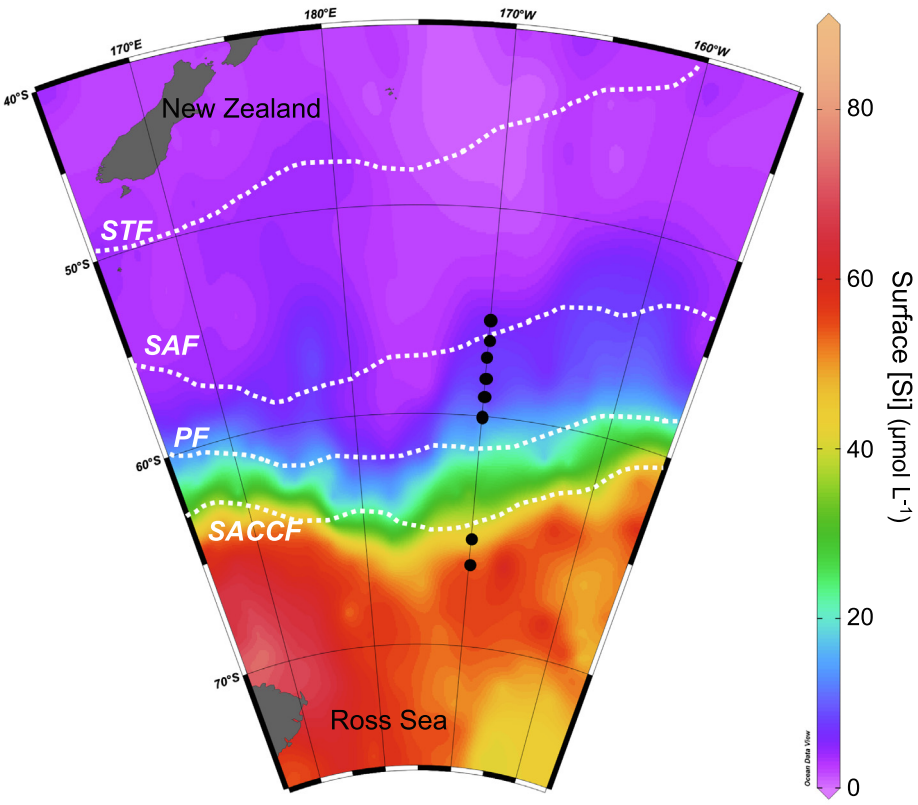

Fig. 1. Map of the SNOWBIRDS section across the Southern Ocean along 170°W with main hydrographic fronts (from Orsi et al., 1995). From south to north, the Southern ACC Front (SACCF), the Polar Front (PF) the Sub-Antarctic Front (SAF) and the Sub-Tropical Front (STF). The colors represent the mean annual surface silicic acid concentration ([Si], in µmol L^{-1}).

frustules from the euphotic zone as used by Demarest et al. (2009), show no isotopic fractionation during dissolution in aqueous NaOH (Wetzel et al., 2014). Moreover, sinking and core top $bSiO_2$ in the deep ocean and in lakes bear $\delta^{30}Si$ values that are coherent with that of $bSiO_2$ in the mixed layer (Closset et al., 2015; Egan et al., 2012; Panizzo et al., 2016).

In marine sediments, processes that characterize early silica diagenesis have been shown to fractionate silicon isotopes (Tatzel et al., 2015; Geilert et al., 2016). Due to the expression of kinetic isotope effects, the light ^{28}Si isotope reacts faster than the heavier ^{30}Si isotope (Fry, 2006). The formation of secondary authigenic minerals through direct silica precipitation from saturated solutions results therefore in an enrichment of ^{30}Si in the dissolved phase and a preferential incorporation of ^{28}Si in the solid phase (e.g. Delstanche et al., 2009; Geilert et al., 2014; Roerdink et al., 2015). The isotopic fractionation of Si isotopes during authigenic silica precipitation ($^{30}\varepsilon_{Auth}$) has been estimated to be −1.6 to −2‰ (Ziegler et al., 2005; Meheut et al., 2007; Ehlert et al., 2016).

Burial of the $bSiO_2$ that settles on the sediment surface is controlled by $bSiO_2$ dissolution, its re-precipitation and its adsorption to sediment. Unique isotopic fractionations during these processes could lead to predictable shifts in the isotopic composition of $bSiO_2$ dissolved in sediment pore waters such that the determination of pore water $\delta^{30}Si$ values can help decipher the complex Si cycle in surface sediments. These processes also set the isotopic composition of the dissolved Si entering the deep sea through sediment efflux, a key input of silicic acid to the global ocean (DeMaster, 1981; Frings, 2017; Tréguer et al., 2021). However, we still lack a comprehensive understanding of the processes controlling the flux of dissolved Si from the superficial sediments to the bottom waters and those governing the Si isotopic composition of both pore water and opal preserved within deep oceanic sediments.

This study quantifies the efflux of Si from sediments beneath the major latitudinal zones in the Pacific sector of the Southern Ocean and evaluates the processes controlling the $\delta^{30}Si$ of pore waters and of $bSiO_2$ during early diagenesis. Our goal is to better understand how sediment processes may affect the use of the $\delta^{30}Si$ proxy for paleoreconstructions of upper ocean nutrient dynamics and productivity.

2. MATERIAL AND METHODS

2.1. Study area

This study is part of the SNOWBIRDS (Silicon and Nitrogen Observed in the Water column Biologic Isotope Records During Sedimentation) project that took place in January – February 2017 along a transect from 67°S to 55°S latitude, 170°W longitude, spanning the three main hydrographic zones of the Southern Ocean (Fig. 1, Table 1).

Table 1
Pore water and overlaying seawater Si concentration ($[Si]_{pw}$, ($[Si]_{overlay}$), $bSiO_2$ observed solubility or equilibrium concentration ($[Si]_{eq}$), $bSiO_2$ content and isotopic compositions of pore water ($\delta^{30}Si_{pw}$), $bSiO_2$ ($\delta^{30}Si_{BSi}$) and lithogenic silica ($\delta^{30}Si_{LSi}$) at the seawater-sediment interface (0–1 cm). * Overlaying seawater Si concentrations likely contaminated with pore water Si during sample manipulation. Although displayed in figures and tables, these concentrations were not used in any calculation in this study.

Zone	Lat	Depth	$[Si]_{overlay}$	$[Si]_{pw}$	$[Si]_{eq}$	J_{sw}	$\delta^{30}Si_{pw}$		$bSiO_2$	$\delta^{30}Si_{BSi}$		$\delta^{30}Si_{LSi}$	
	∘S	m	μmol L^{-1}	μmol L^{-1}	μmol L^{-1}	mmol m^2 yr^{-1}	‰	*sd*	wt%	‰	*sd*	‰	*sd*
AZ	67	3733	98	345	411	235	0.54	*0.00*	23.62	0.71	*0.06*	−0.07	*0.07*
	66	2700	121	355	616	142	0.67	*0.09*	19.48	0.75	*0.05*	−0.08	*0.10*
PFZ	60	3793	443*	534	942	203	1.00	*0.07*	37.91	1.59	*0.04*	−0.04	*0.01*
	59	4750	303*	466	772	320	1.27	*0.04*	48.99	1.55	*0.09*	0.13	*0.08*
	58	4490	136	315	673	90	1.18	*0.00*	25.72	1.51	*0.08*	n.a.	*n.a.*
	57	4668	144	225	532	67	1.42	*0.08*	21.20	1.16	*0.02*	n.a.	*n.a.*
	56	4375	125	193	544	56	1.34	*0.09*	10.82	1.27	*0.03*	n.a.	*n.a.*
SAZ	55	4645	119	175	522	54	1.20	*0.05*	12.59	1.00	*0.07*	−0.19	*0.05*

A total of eight sediment cores were collected (from 2700 m to 4750 m depth) along the transect. Two cores were collected beneath the Antarctic Zone (AZ), defined as the southernmost region of the Southern Ocean (from 67°S to 61°S along the transect), where biological production is dominated by diatoms. In this region, the biological production is not limited by macronutrient availability, but rather controlled by irradiance and iron concentrations (Trull et al., 2001). The AZ is usually characterized by high $bSiO_2$ export to the ocean interior, and ultimately high $bSiO_2$ accumulation rates in sediments (DeMaster, 1981). The Polar Front (PF), located between 61°S and 62°S along the SNOWBIRDS transect, corresponds to the major locus of $bSiO_2$ accumulation in the marine environment (Chase et al., 2003) and is identified as the opal belt. Unfortunately, we were unsuccessful in coring the high opal sediments. To the north, the Polar Front Zone (PFZ) lies between the PF and the Sub-Antarctic Front (SAF). Five sediment cores were collected in the PFZ (from 61°S to 56°S), where silicic acid concentrations display the highest meridional gradient with an overall change in DSi of >40 μmol L^{-1} (Fig. 1; Brzezinski et al., 2001; Frank et al., 2000) in surface waters. Finally, one sediment core was collected north of 56°S in the Sub-Antarctic Zone (SAZ), where cold nutrient-rich polar waters transition to the warm nutrient-poor subtropical waters at the Sub-Antarctic Front (SAF). In this zone, nitrate and phosphate concentrations remain moderately high, but silicic acid concentrations are low throughout the year (1–4 μmol L^{-1}; Trull et al., 2001), limiting diatoms and favoring non-siliceous autotrophic organisms such as coccolithophorids (Kopczynska et al., 2001; De Salas et al., 2011).

2.2. Sampling and processing

Sediment cores were collected using an OSIL Mega Corer to acquire up to 12 short cores (each typically around 20 cm in length). This system was able to preserve the sediment–water interface. Dating of planktonic foraminifera from the 0–1 cm depth interval of the cores were performed to verify the ages of the uppermost sediment samples (see details in Robinson et al., 2020). The calibrated radiocarbon ages indicate that the surface sediments in each zone was mid- to late Holocene in age consistent with ages published by Chase et al. (2003) along the same transect. Samples for bottom water analysis were taken from the supernatant water above each core. Processing of sediments was conducted aboard ship immediately after recovery by first gently siphoning the overlying seawater then extruding the sediment and sectioning at 0.5 to 2 cm intervals with the highest resolution close to the sediment surface. Pore water (typically between 5 and 15 ml per sample) was collected by transferring each sediment section to a 50 ml centrifuge plastic tube and subsequently centrifuging at 4500 rpm for 20 min. Supernatants were carefully removed and filtered through 0.2 μm polycarbonate filters. Pore water samples were then diluted with deionized water and stored in the dark for later isotope analysis. The sediments remaining after centrifugation were frozen for further analysis on shore. The entire operation was completed within 2 hours after the retrieval of the cores which is a timeframe where no critical change in pore water silicic acid profiles is observed (Hendry et al., 2019).

2.3. Silicic acid and $bSiO_2$ concentrations

Pore water silicic acid concentration (referred to as [Si] in figures) was measured colorimetrically on-board ship immediately after sampling and also post-expedition at UCSB using standard photometric techniques (Brzezinski and Nelson, 1995). Samples dilution was adjusted to conform to the matrix of the standards solutions used in the calibration curve. The precision and reproducibility of the method were assessed using repeat measurements of an in-house standard solution (8.45 ± 0.63 μmol L^{-1}, n = 43) and duplicate sample measurements and averaged 7%.

The $bSiO_2$ mass fraction (or $bSiO_2$ content, wt%) of sediment samples was determined using a sequential wet alkaline extraction method adapted from DeMaster (1981). A known weight of the freeze-dried sample material was treated with 1 M Na_2CO_3 at 85 °C for up to 8 h to extract the opal fraction. Aliquots were taken every hour and neutral-

ized immediately with HCl. The increase in dissolved silicon was monitored colorimetrically using the same method as for silicic acid concentrations determination and the $bSiO_2$ content was evaluated as described in DeMaster (1981). Typical analytical errors of the overall procedure derived from the average of standard deviations of repeated $bSiO_2$ measurements ranged from 0.05 to 8%.

2.4. Biogenic and lithogenic silica extraction for isotopes

Sample preparation for Si isotope analyses in sediments was carried out at University of Rhode Island (URI) where freeze-dry sediments were first homogenized and treated with 1 M HCl to remove carbonate material. Biogenic silica was then separated from the lithogenic fraction following the method of Morley et al. (2004). Briefly, sediments were sieved using a 63 μm mesh sieve and fine clay particles (grain size < 2 μm) were separated from the sediment by settling for 12 h. This size fraction (2–63 μm) was chosen because it contained a high abundance of frustules from different diatoms species with minor contribution by other $bSiO_2$ material such as fragments of Rhizaria or sponge spicules (Egan et al., 2012). Diatoms were subsequently separated from the remaining lithogenic fraction using sodium polytungstate density centrifugation. The heavy liquid purification method was repeated until a clean opal fraction was obtained as indicated by inspection using light microscopy. Pure diatom samples and associated lithogenic fractions were rinsed, dried and stored separately until further isotopic analysis.

2.5. Silicon isotopes analysis

Samples for pore water isotopic measurements ($\delta^{30}Si_{pw}$) were processed at LOCEAN-IPSL (Paris, France). They were first preconcentrated using a procedure adapted from the MAGIC method (Karl and Tien, 1992; Reynolds et al., 2006). Briefly, silicic acid was co-precipitated in two steps with brucite ($Mg(OH)_2$) by adding 2% (v:v), followed by 1% (v:v) of 1 M NaOH to the seawater sample. The precipitate was then recovered by centrifugation and dissolved with 1 M HCl. Si recovery was monitored by checking systematically that no detectable amount of silicic acid remained in the supernatant after co-precipitation and centrifugation. After preconcentration, samples were purified through a cation-exchange column (BioRad cation-exchange resin DOWEX 50W-X12, 200 to 400 mesh) using the protocol described in Georg et al. (2006). The purified Si solutions were analyzed on a Thermo Neptune$^+$ multi-collector inductively coupled plasma mass spectrometer (MC-ICPMS; LSCE-IPSL, Gif-sur-Yvette, France) in dry plasma mode with Mg external doping to correct for the mass bias (Cardinal et al., 2003; Abraham et al., 2008). Blank levels were below 1% of the main signal and were subtracted from each sample and standard analysis. All measurements were performed on the interference-free left side of the peak (Abraham et al., 2008). Typical analytical conditions are provided in Table S2. The $\delta^{29}Si$ and $\delta^{30}Si$ values for all standards and samples were compared to the mass-dependent isotopic fractionation line (Fig. S1) and the few samples falling outside of its analytical error were excluded from the final dataset. Numerous analyses of the secondary reference material diatomite yielded a $\delta^{30}Si$ value of $+1.28 \pm 0.05$‰ (1 sd, n = 128) in good agreement published interlaboratory comparisons ($\delta^{30}Si = +1.26 \pm 0.10$‰, 1 sd, n = 82; Reynolds et al., 2007).

Samples for the isotopic measurements of the diatom ($\delta^{30}Si_{BSi}$) and lithogenic ($\delta^{30}Si_{LSi}$) fractions, were analyzed at UCSB (Santa Barbara, California). Briefly, SiO_2 was converted to $BaSiF_6$ by dissolution in HF, addition of CsCl to obtain Cs_2SiF_6 and later addition of a solution of BaCl and HF to convert Cs_2SiF_6 to $BaSiF_6$. Si isotopes were then analyzed on the NuSil IRMS with SiF_4 generated through the thermal decomposition of $BaSiF_6$. Samples were run against cryogenically purified commercial SiF_4 gas using a sample-standard bracketing approach. The final $\delta^{30}Si$ value was calculated according to Paul et al. (2007) using a multiple-point normalization procedure, that is, based on the linear relationship between the consensus values and measured $\delta^{30}Si$ values of two or more reference standards (in this study NBS28, Big Batch, and Diatomite) to achieve a more constrained calibration. Repeated measurement of the reference material Diatomite ($+1.23 \pm 0.06$‰, 1 sd, n = 46) is in good agreement with $\delta^{30}Si$ values found in the literature (Reynolds et al., 2007).

The $\delta^{30}Si$ values of pore water, $bSiO_2$, and lithogenic silica are given as $\delta^{30}Si_{pw}$, $\delta^{30}Si_{BSi}$ and $\delta^{30}Si_{LSi}$, respectively. Error bars shown in the figures correspond to the analytical reproducibility of duplicates of samples measured on separate days.

2.6. Analytical intercomparison between UCSB and IPSL

The combination of the different methods used for chemical sample preparation, including preconcentration and purification methods, and isotopic analysis on different mass-spectrometers such as the Neptune MC-ICP-MS (Thermo Fisher™, Germany) used at IPSL laboratories, and the NuSil and Nu Perspective IRMS (Nu Instruments, UK) used at UCSB, can cause inter-laboratory differences (e.g. Brzezinski and Jones, 2015). External reproducibility (1 sd) of the reference material Diatomite analyzed by both laboratories, 0.05‰ and 0.06‰ for IPSL and UCSB, respectively are similar to those obtained during the inter-laboratory comparison of Si isotopes in seawater (Grasse et al., 2017) and in pure solid siliceous materials (Reynolds et al., 2007). The mean results for Diatomite measured in both institutes are in very good agreement (<±0.1‰ difference; with $\delta^{30}Si = +1.23 \pm 0.12$‰, 2 sd, n = 46, and $\delta^{30}Si = +1.28 \pm 0.1$‰,2 sd, n = 128 for UCSB and LOCEAN-IPSL, respectively) confirming the previously published conclusion that there is no systematic offset between MC-ICP-MS and IRMS (Grasse et al., 2020; Brzezinski et al., 2021).

3. RESULTS

3.1. Particulate silica content and isotopic composition

Profiles of $bSiO_2$ content $\delta^{30}Si_{BSi}$ and $\delta^{30}Si_{LSi}$ were measured in 5 of our 8 cores, covering the 3 zones of the South-

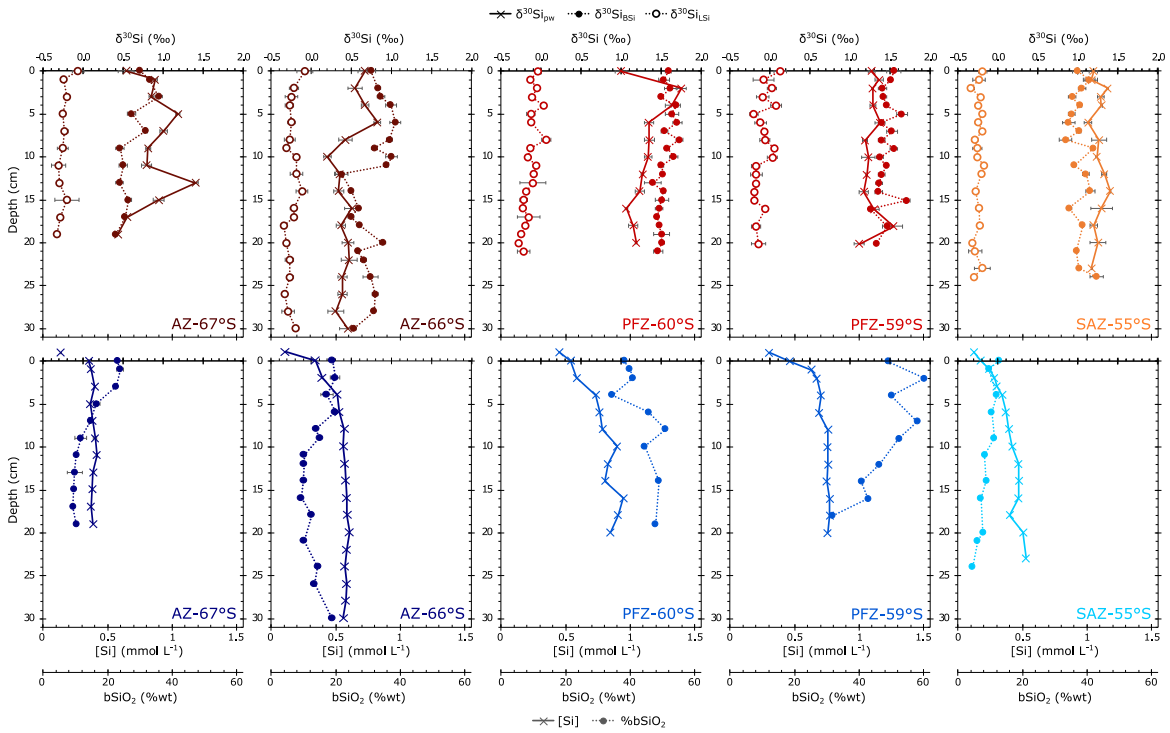

Fig. 2. Depth profiles of pore water silicic acid concentration ([Si], in mmol L^{-1}) and isotopic composition (in ‰) along with $bSiO_2$ content (in %), $bSiO_2$ isotopic composition (in ‰, colored dotted lines), and LSi isotopic composition (in ‰).

ern Ocean (Fig. 2). The $bSiO_2$ content varied amongst sites, being more abundant in the mid-stations of the transect, consistent with previous published values along the same transect (see Sayles et al., 2001; Chase et al., 2003). At the seawater-sediment interface, $bSiO_2$ content was highest in the southern part of the PFZ (up to 49 wt% at 59°S) and decreased northward to values around 13 wt% in the SAZ (Table 1). The two AZ cores displayed similar $bSiO_2$ contents to those in the SAZ with around 20 wt% in the upper first cm of the sediment. Unfortunately, we were not able to obtain sediment cores between 60°S and 66°S. The sediments close to the PF (around 61°S) were expected to be nearly pure biogenic oozes where $bSiO_2$ is by far the most abundant component. The $bSiO_2$ content was significantly higher in the uppermost part of both AZ cores and decreased by a factor of two between 5 and 10 cm and remained low at the bottom of the cores (Fig. 2).

Variations in the isotopic composition of $bSiO_2$ at the seawater-sediment interface among cores matched the spatial pattern of variation in $bSiO_2$ content with higher $\delta^{30}Si_{BSi}$ near the PF (up to +1.59 ± 0.04‰) that progressively decreased northward to +1.00 ± 0.07‰ in the SAZ (Table 1). In the AZ, the $\delta^{30}Si_{BSi}$ was significantly lower (+0.71 and +0.75‰ at 67°S and 66°S, respectively) compared to stations north of the PF. North of the PF, the downcore $\delta^{30}Si_{BSi}$ profiles did not vary significantly with depth (Fig. 2). They averaged +1.50 ± 0.11‰ and +1.03 ± 0.11‰ in the PFZ and SAZ, respectively. In contrast, $\delta^{30}Si_{BSi}$ values were on average 0.3‰ higher in the uppermost part of the AZ cores matching the pattern of variations observed in the $bSiO_2$ content with higher $\delta^{30}Si_{BSi}$ corresponding to higher $bSiO_2$ content.

The $\delta^{30}Si_{LSi}$ was remarkably homogeneous among sites and also within sediment depth (Fig. 2). It ranged from −0.34‰ to +0.13‰ and averaged −0.18 ± 0.10‰ across all cores. This value is not different from the average Si isotopic composition of the upper continental crust (−0.25 ± 0.08‰; Savage et al., 2013) which is the major source of Si to the ocean and is likely representative of the majority of the lithogenic silica fraction in our samples. Interestingly, the two cores located in the PFZ (59°S and 60°S) displayed a slightly higher $\delta^{30}Si_{LSi}$, averaging −0.11 ± 0.10‰, compared to the other zones (−0.24 ± 0.07‰ and −0.24 ± 0.05‰ in the AZ and SAZ, respectively). In the PFZ, the amount of lithogenic material remaining after heavy liquid separation was so small that the very small fraction of biogenic silica remaining after separation, insignificant compared the amount of lithogenic material in the other zones, could represent enough material to contaminate the lithogenic fraction in the PFZ and slightly affect the $\delta^{30}Si_{LSi}$. We thus attribute this small variability to the incomplete separation of the biogenic and lithogenic fractions.

3.2. Pore water silicic acid concentrations and isotopic composition

The range in average pore water silicic acid concentrations between stations was large compared to that in the overlying bottom water. Silicic acid concentrations in the overlying bottom water exhibited the typical range for

AABW (on average 124 ± 16 μmol L^{-1}, except for two stations in the PFZ with concentration >300 μmol L^{-1}, where we suspect mixing and contamination with silicic acid rich pore water during sampling). The concentrations in the first centimeter of sediment ranged from 175 μmol L^{-1} in the northern part of the transect to 535 μmol L^{-1} close to the Polar Front (Table 1). Sharp gradients with pore water concentrations increasing with depth were present in all the profiles and were most pronounced in the first 5 cm of the cores (Fig. 2). The down-core trends of pore water Si concentrations generally fit an exponential curve (see Fig. S2), where silicic acid increased asymptotically to a maximum average concentration between 400 and 500 μmol L^{-1} in the AZ, between 500 and 900 μmol L^{-1} in the PFZ and between 400 and 500 μmol L^{-1} in the SAZ in the deeper part of the cores. In the southern part of the transect (from 67°S to 59°S), the silicic acid concentration of pore waters remained constant below 10 cm indicating apparent equilibrium.

The range of $\delta^{30}Si_{pw}$ values was similar to the Si isotopic composition of $bSiO_2$ preserved in the cores, suggesting that the distribution of $\delta^{30}Si_{pw}$ is mostly controlled by the dissolution of $bSiO_2$ within the sediment. North of the PF, the downcore profiles of $\delta^{30}Si_{pw}$ did not vary systematically with depth or sampling site, except for the station at 60°S where there was a slight trend of decreasing $\delta^{30}Si_{pw}$ with core depth (Fig. 2). The mean $\delta^{30}Si_{pw}$ for these cores was +1.28 ± 0.14‰ with most of the variation due to measurement error and from natural variability in the core itself. In contrast, the $\delta^{30}Si_{pw}$ of the two cores located in the AZ exhibited a significantly different $\delta^{30}Si_{pw}$ profiles compared to the other stations (Fig. 2). At 66°S, the highest $\delta^{30}Si_{pw}$ values occurred in the uppermost part close to the seawater-sediment interface (+0.68 ± 0.11‰ from 0 to 6 cm), then $\delta^{30}Si_{pw}$ decreased progressively towards values as low as +0.20 ± 0.04‰ at 10 cm and stabilized around + 0.40 ± 0.06‰ in the deeper part of the core. At 67°S, the $\delta^{30}Si_{pw}$ displayed a strong variability with depth ranging from +0.43 ± 0.07‰ at the bottom of the core to +1.40 ± 0.03‰ in the middle part of the core.

4. DISCUSSION

4.1. Seawater-sediment interface dynamics and benthic Si fluxes

4.1.1. Silicon diffusive flux to the ocean

All pore water silicic acid concentrations are higher than those of the overlying seawater, which will drive a diffusive flux of silicic acid out of the sediment (Fig. 2). Benthic fluxes are best measured *in situ* at the sediment–water interface, however, high resolution accurate concentration measurements of pore water gradients can be used to estimate silicic acid fluxes to the bottom water (e.g. Sayles et al., 2001). The silicic acid molecular diffusive flux through the sediment–water interface (J_{sw} across the first cm of sediment, in mmol m^{-2} yr^{-1}) can be calculated using Fick's First Law modified for sediments and applied to an exponential fit to the pore water silicic acid concentration profiles (see Fig. S2) following the equation:

$$J_{sw} = -\phi D_s \frac{\partial c}{\partial z} \quad (2)$$

Where ϕ is the mean porosity in the top core (dimensionless value ranging from 0 to 1); D_s refers to the diffusion coefficient in the sediment; and $\frac{\partial c}{\partial z}$ is the concentration gradient between the 0–1 cm fitted value of pore water and the bottom water. Porosity values (ϕ) have not been measured in our sediment cores. However, surface sediment porosities varying from 0.78 to 0.89 (avg. 0.86 ± 0.04) were previously determined on cores collected along the same transect (AESOPS program; Sayles et al., 2001). We therefore assume uniform porosity in the first 0–1 cm of the sediments for the flux calculations with an averaged value of 0.86 for all investigated sites. The diffusion coefficient of Si in the first 0–1 cm of the sediment (in m^2 s^{-1}) was calculated using:

$$D_s = \frac{D_m}{\theta^2} \quad (3)$$

Where D_m refers to the molecular diffusion coefficient of Si in seawater ($D_m = 4.59 \times 10^{-10}$ m^2 s^{-1} for a temperature of 0 °C (Schulz, 2006); and θ^2 is the tortuosity in the first 0–1 cm of the sediment, a term used to describe the degree of the sinuous diffusion path (or "deviations") around each sediment particle ($\theta^2 = 1.3$ such as in Schulz, 2006 and references therein).

The calculated benthic diffusive fluxes of silicic acid from sediments to seawater (J_{sw} in Table 1), range from 53 to 320 mmol m^{-2} yr^{-1} consistent with previously obtained values along the same transect (from 100 to 409 mmol m^{-2} yr^{-1} at the corresponding stations, see Sayles et al., 2001). These fluxes show a clear zonal trend, with a maximum near the PF and the lowest values occurring at the northern extreme of the transect. This zonal trend matches closely the spatial distribution of the $bSiO_2$ content of the sediment and, not surprisingly, of silicic acid concentrations in pore water ($R^2 = 0.73$ and $R^2 = 0.67$, respectively, Fig. 3), indicating that the dissolution of $bSiO_2$ and subsequent benthic diffusive flux are controlled by $bSiO_2$ content in the first few centimeters of the sediments. This suggests that high benthic diffusive fluxes of silicic acid occur in sediments underlying areas of high productivity in the Southern Ocean pelagic environment. Interestingly, except in the AZ where the $\delta^{30}Si_{pw}$ is significantly lower than values in the other zones, the isotopic composition of this diffusive flux does not differ from the averaged isotopic composition of bottom water (1.25 ± 0.23‰, Sutton et al., 2018; see Table 1) and will likely have no significant effect on the latter.

4.1.2. Silicon recycling in the sediments

Dissolution of $bSiO_2$ in sediments must also be evaluated to understand the Si isotope dynamics in the sediments. Van Cappellen and Qiu (1997) showed that the rate of $bSiO_2$ dissolution in marine sediments is strongly and non-linearly dependent on the magnitude of deviation of seawater from saturation in Si. The apparent saturation, referred to here as the equilibrium solubility of $bSiO_2$ (S_{eq}), can be estimated from an exponential fit to the pore water silicic acid concentration profiles (Fig. S2). When the gradi-

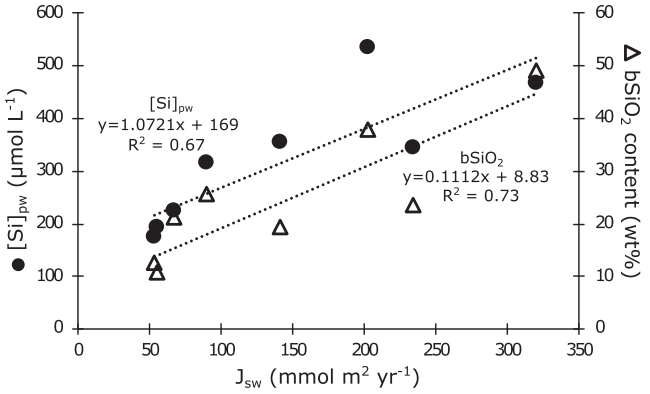

Fig. 3. Relation between Si diffusive flux (J_{sw}, in mmol m^2 yr^{-1}), silicic acid concentration in pore water measured in the first 0–1 cm ([Si], in µmol L^{-1}) and $bSiO_2$ content in the sediments (in wt%).

ent of pore water silicic acid concentration is low (when the curve reaches a plateau) the system reaches a steady state, i.e. the dissolution of $bSiO_2$ either stops or is balanced by another process such as reverse weathering (see Section 4.2.3) and the pore water silicic acid concentration reflects the equilibrium solubility associated with the core.

Along the SNOWBIRDS transect, calculated S_{eq} varies by a factor of two, with a maximum near the PF and a decreasing trend both northward and southward (Table 1). With the exception of station located at 67°S, these values are comparable to published estimates of $bSiO_2$ solubility in sediments with a high $bSiO_2$ content in the Southern Ocean (e.g. Rabouille et al., 1997; Dixit et al., 2001). Variations of the solubility of $bSiO_2$ in sediments is not uncommon. It has been shown that the S_{eq} given by the asymptotic increase of the pore water silicic acid profile does not necessarily reflect the true solubility of $bSiO_2$ (Van Cappellen and Qiu, 1997). Indeed, the solubilities measured in the superficial sediment may already be lower by about 100–150 µmol L^{-1} compared to the solubility of fresh diatoms collected in the surface waters of the Southern Ocean (estimated as ca. 1000 µmol L^{-1}; Van Cappellen and Qiu, 1997). Moreover, $bSiO_2$ solubility depends on a variety of factors including the specific surface area of the particle, its aluminum content, and ambient pressure, pH and temperature (Van Cappellen et al., 2002).

The shape of the curves displayed in Fig. 2 and Fig. S2 can also be used as a qualitative indicator of the sediment horizon where most of $bSiO_2$ dissolution occurs. Even though other processes, such as reverse weathering that can counteract $bSiO_2$ dissolution, have the potential to affect the shape of the pore water silicic acid concentration profile, the depth zone where the asymptote is approached (i.e. the curvature of the profile) likely reflects the depth where the $bSiO_2$ dissolution rate starts to slow down when the system reaches equilibrium. In our study, this curvature differs strongly between the southern and northern part of the transect. The locus of $bSiO_2$ dissolution seems to occur deeper in the SAZ compared to the AZ or stations located south of 59°S. This may also reflect the effect of reverse weathering that consume pore water silicic acid to precipitate authigenic alumino-silicates, preventing the system to locally reach S_{eq} and therefore allowing $bSiO_2$ to dissolve deeper in the sediment core.

The combination of these two observations suggests strong potential spatial variations of the $bSiO_2$ dissolution rates along the transect, with relatively high rates in the AZ reaching a maximum around the PF and decreasing northward to reach a minimum in the SAZ. This is consistent with the benthic diffusive fluxes estimated from pore water silicic acid profiles and implies that the dissolution of $bSiO_2$ in the sediments and the spatial variations of the equilibrium solubility both exert a strong control on pore water concentrations and diffusive Si flux to the deep ocean observed during SNOWBIRDS.

This is also consistent with observations from other studies along the exact same transect (AESOPS program, Sayles et al., 2001; Chase et al., 2003) and along a transect located in the Indian Sector of the Southern Ocean (ANTARES I program; Rabouille et al., 1997; Van Cappellen and Qiu, 1997). Sediment compositions investigated during AESOPS revealed a bimodal distribution of the lithogenic material, being greatest at the southern and northern extremes of the transect. These studies postulated that the highest lithogenic burial in the south reflected the contribution of ice rafted debris at these high latitudes while at the northern stations, fine-grained material eroded from the sea floor to the west (possibly from the Campbell Plateau) were advected by currents to the northern portion of the transect. Aluminum (Al) content in the bulk sediments and in the pore water measured in the Indian Sector of the Southern Ocean during ANTARES I increased from south to north (from 0.5 to 6.5 wt% Al of the dry solids; Rabouille et al., 1997). It has been suggested that higher Al concentration in the sediments and pore water likely decreased the solubility of $bSiO_2$ through ionic substitution within the silica structure. Although sediment composition was not investigated in our study, nor Al content measured, enhanced lithogenic burial rich in aluminum-bearing detritus certainly occurred at the extremities of the transect during SNOWBIRDS and may explain the lower $bSiO_2$ observed solubility (Si_{eq}, Table 1) observed in the SAZ or at 67°S in the AZ.

4.2. Insights into controls on the pore water isotopic composition

4.2.1. The dissolution of biogenic silica

As already suggested in previous studies on the Peru and Greenland continental margins (Ehlert et al., 2016; Ng et al., 2020), we hypothesize that the magnitude of the benthic Si flux and its isotopic composition are mainly controlled by the rate of dissolution of $bSiO_2$. Due to its relatively high solubility in seawater most of the $bSiO_2$ deposited on the seafloor dissolves rapidly in the reactive surface layer of the sediment (<10 cm) where the concentration of silicic acid in pore water is lower. The observed exponential increase in pore water silicic acid concentration, as well as the $\delta^{30}Si_{pw}$, in all the sediment cores of our study are therefore likely primarily controlled by the dissolution of $bSiO_2$. Indeed, within the cores, $\delta^{30}Si_{BSi}$ varies between +0.38 ± 0.07‰ and +1.73 ± 0.04‰ and matches closely the range of variations of the $\delta^{30}Si_{pw}$ (from +0.20 to +1.75‰). This is especially true at station 60°S, 59°S and 55°S where $\delta^{30}Si_{pw}$ and $\delta^{30}Si_{BSi}$ show no differences (see Fig. 2).

The relationship between $\delta^{30}Si_{pw}$ and $\delta^{30}Si_{BSi}$ also suggests that there is no apparent isotopic fractionation during $bSiO_2$ dissolution. If isotopic fractionation of Si isotopes occurs during the dissolution of $bSiO_2$ with a $^{30}\varepsilon_{Diss} = -0.55$‰ favoring the release of the lighter isotopes to pore water (Demarest et al., 2009), then the $\delta^{30}Si_{pw}$ value should be 0.55‰ lower than the opal value assuming that all diatoms dissolve congruently. Moreover, the $\delta^{30}Si_{BSi}$ and $\delta^{30}Si_{pw}$ values should both concomitantly increase with depth in the sediment as more $bSiO_2$ is dissolved and a significant fraction of Si is removed from the solid phase. Neither phenomenon is observed. In fact, some stations (e.g. at 67°S and 55°S) $\delta^{30}Si_{pw}$ values are consistently higher than their respective $\delta^{30}Si_{BSi}$ values, indicating that the pore waters are enriched with the heavier Si isotopes rather than the light isotopes as expected from the estimated isotopic fractionation during dissolution. In the same way, the lack of an increasing nor decreasing trend in the $\delta^{30}Si_{LSi}$ values (Fig. 2) suggest that there is no apparent isotopic effect during the dissolution of the lithogenic silica fraction in the sediments.

Additional insight into the processes controlling $\delta^{30}Si_{pw}$ can be gained from deviations from a simple mixing model between dissolving sedimentary opal and the overlying seawater. Assuming that the $\delta^{30}Si_{pw}$ in the sediment is only controlled by a conservative mixing between two distinct end-members (here the dissolution product of $bSiO_2$ and the bottom water mass), pore water samples should display a linear relationship between the concentration and isotope composition of silicic acid (see de Souza et al., 2012b for conservative mixing of water masses in the deep Atlantic Ocean). Deviations of the measured $\delta^{30}Si$ from that predicted by strict conservative mixing would indicate the influence of one or more additional processes in the control of the $\delta^{30}Si_{pw}$ (see Fig. 4 and e.g. Geilert et al., 2020). Here, we used a conservative mixing between the deep-water mass (AABW) and fluids originating from $bSiO_2$ dissolution as follows:

$$\delta^{30}Si_{mix} = \frac{f_{AABW}\delta^{30}Si_{AABW}[Si]_{AABW} + (1 - f_{AABW})\delta^{30}Si_{BSi}S_{eq}}{f_{AABW}[Si]_{AABW} + (1 - f_{AABW})S_{eq}} \quad (4)$$

Where $\delta^{30}Si_{AABW}$ and $[Si]_{AABW}$ are the respective AABW silicic acid Si isotope composition and concentration (+1.24 ± 0.02‰ and 122 µmol L^{-1}, Cardinal et al., 2005; de Souza et al., 2012a, 2012b), $\delta^{30}Si_{BSi}$ here is the isotopic composition of core top diatoms for each sediment core

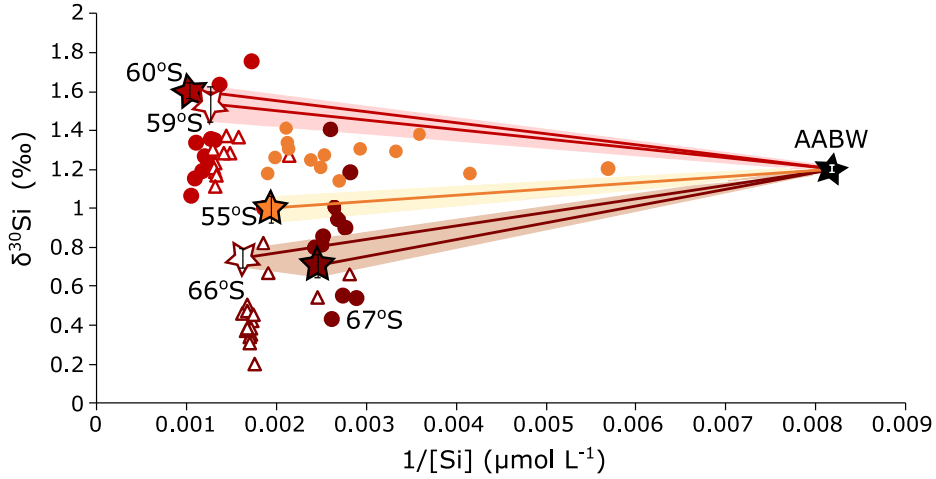

Fig. 4. Pore water isotopic composition vs. the inverse silicic acid concentration (1/[Si]) for the different cores. Lines represent mixing curves between the AABW and the surface $bSiO_2$ $\delta^{30}Si$ value for the different zones: Antarctic Zone in brown (circles are for station 67°S, open triangles for stations 66°S), Polar Front Zone in red (circles are for station 60°S and open triangles for station 59°S) and Sub-Antarctic Zone in orange circles. Colored surfaces represent the propagated uncertainty of the predicted values for each zone, AZ in brown, PFZ in red and SAZ in orange. End-members (stars) are AABW (black), surface $bSiO_2$ at 67°S and 66°S (brown and open brown stars); surface $bSiO_2$ at 60°S and 59°S (red and open red stars); and surface $bSiO_2$ at 55°S (orange star).

that corresponds to the least altered $bSiO_2$ relative to that that just reached the sediment and S_{eq} is the concentration corresponding to the equilibrium concentration with respect to $bSiO_2$ dissolution or equilibrium solubility (Table 1, Fig. S2).

Except in the SAZ, where there is a clear mixing of AABW in the sediment likely associated with some degree of bio-irrigation, pore water silicic acid concentrations are grouped close to the $bSiO_2$ end-member of the mixing line between $bSiO_2$ and AABW (Fig. 4), confirming the strong control of the $bSiO_2$ dissolution on the pore water silicic acid profiles. Interestingly, pore water Si isotopic composition of all sites deviate from mixing curves between the deep-water column and fluids originating from $bSiO_2$ dissolution (Fig. 4) and are obviously affected by additional processes. By calculating the deviation of measured $\delta^{30}Si$ values from those expected from pure mixing of the two end-members ($\Delta^{30}Si_{dev} = \delta^{30}Si_{measured} - \delta^{30}Si_{predicted}$), we can investigate the influence of these additional processes on the control of the isotopic composition of pore waters along the SNOWBIRDS transect. Note that this approach of predicting $\delta^{30}Si_{pw}$ assuming a simple 2 end-member mixing implies that the end-member values do not change with time. This assumption is likely an oversimplification for sediments since we expect $\delta^{30}Si_{BSi}$ to change with time (or sediment depth horizon) depending on the degree of silicic acid consumption in surface waters by diatoms. However, except in the AZ where $\delta^{30}Si_{BSi}$ values were on average 0.3‰ higher in the uppermost part of the cores, the downcore $\delta^{30}Si_{BSi}$ profiles in the PFZ and SAZ did not vary significantly with depth (Fig. 2). Consequently, we can assume that $\Delta^{30}Si_{dev}$ values are relatively unbiased for stations located in the PFZ and SAZ, but need to be interpreted more cautiously in the AZ. Therefore, we decided to split the AZ cores into two sections, (i) the uppermost section where we assume that the $\delta^{30}Si_{BSi}$ end-member is approximated by the isotopic composition value of core top diatoms (i.e. the less altered $bSiO_2$ that just reach the sediment, Table 1); (ii) the downcore section, after the measured $\delta^{30}Si_{BSi}$ shift. Here we chose the downcore averaged $\delta^{30}Si_{BSi}$ value as end-member (0.48 ± 0.06‰ and 0.63 ± 0.15‰ for 67°S and 66°S, respectively, see Fig. 5).

4.2.2. The dissolution of lithogenic silica

Values of $\Delta^{30}Si_{dev}$ vary widely, but somewhat systematically, among the different cores (Fig. 5), indicating that processes governing the pore water Si isotopic composition differ significantly between latitudes and sedimentation regimes. $\delta^{30}Si_{pw}$ values of the two PFZ stations, as well as station at 66°S in the AZ, deviate from the mixing curve between the AABW and fluids originating from $bSiO_2$ dissolution. They are shifted to lower values ($\Delta^{30}Si_{dev}$ down to −0.6‰), with the exception of the uppermost section of the sediment core located at 60°S which displays positive $\Delta^{30}Si_{dev}$ values (Fig. 5). Assuming that there is no apparent effect of isotopic fractionation of Si isotopes caused by $bSiO_2$ dissolution, the overall negative $\Delta^{30}Si_{dev}$ values observed in the PFZ can be explained by the dissolution of the lithogenic silica fraction, which is generally enriched in ^{28}Si. The high resolution $\delta^{30}Si_{LSi}$ profiles measured in this study allow us to estimate the relative LSi contribution (f_{LSi}) to the observed pore water $\delta^{30}Si$ value using the following equation:

$$X_{pw} \times \delta^{30}Si_{pw} = X_{LSi} \times \delta^{30}Si_{LSi} + X_{pred} \times \delta^{30}Si_{pred} \quad (5)$$

Where X_{LSi} and X_{pred} represent the mole fraction of Si contributed by lithogenic silica and by the pore water silicic acid predicted by the model originating only from the con-

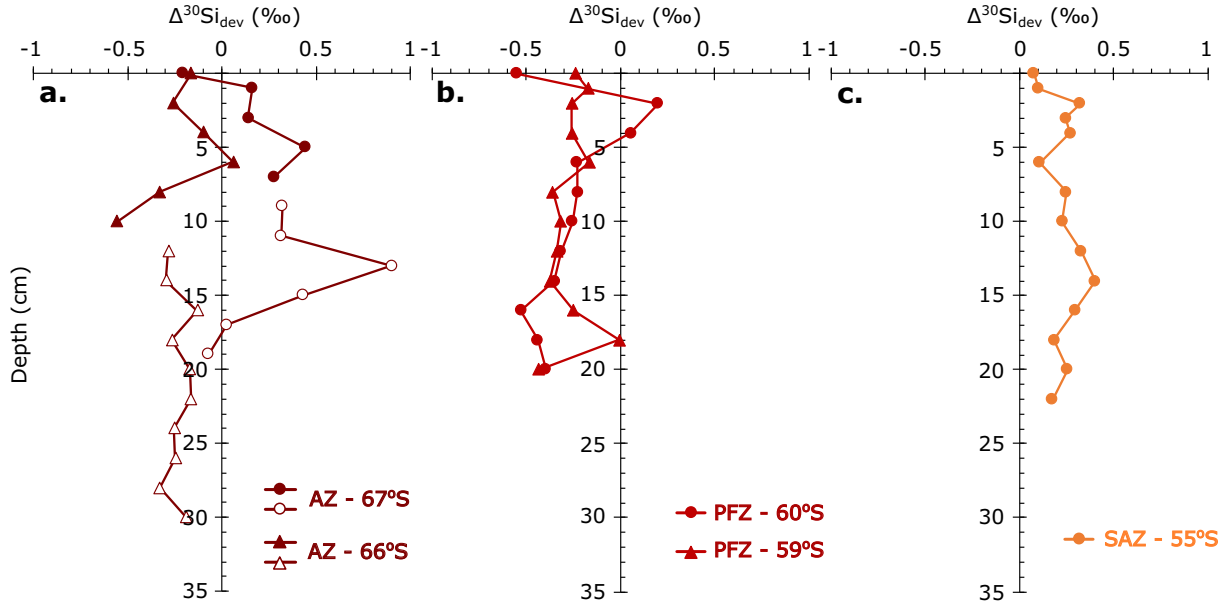

Fig. 5. Deviation of measured $\delta^{30}Si$ values from those expected from pure mixing of the two end-members ($\Delta^{30}Si_{dev} = \delta^{30}Si_{measured} - \delta^{30}Si_{predicted}$) for the different zones, Antarctic Zone in brown, Polar Front Zone in red and Sub-Antarctic Zone in orange. Y axis is the depth in the sediment core (in cm).

servative mixing between AABW and the dissolution of $bSiO_2$, respectively; and where $X_{pred} \times \delta^{30}Si_{pred} = X_{BSi} \times \delta^{30}Si_{BSi} + X_{AASW} \times \delta^{30}Si_{AASW}$. Assuming congruent dissolution, the relative lithogenic silica contribution (f_{LSi}) to the observed pore water Si is defined as:

$$f_{LSi} = \frac{X_{LSi}}{X_{pw}} \quad (6)$$

Combining Eqs. (5) and (6) gives:

$$f_{LSi} = \frac{\delta^{30}Si_{pw} - \delta^{30}Si_{pred}}{\delta^{30}Si_{LSi} - \delta^{30}Si_{pred}} \quad (7)$$

In the PFZ, on average 20 ± 5% and 17 ± 7% at 60°S and 59°S, respectively, of the pore water silicic acid originates from the dissolution of the lithogenic silica fraction while this fraction represents approximately 27 ± 12% of the pore water silicic acid at 66°S.

4.2.3. The precipitation of alumino-silicates through reverse weathering

The $\delta^{30}Si_{pw}$ of the core located in the SAZ and at 67°S in the AZ are generally higher ($\Delta^{30}Si_{dev}$ on average +0.24 ± 0.20‰) compared to the predicted value from a simple mixing, indicating that the pore water has been enriched in the heavy ^{30}Si (Fig. 5). The most likely explanation is that the heavy $\delta^{30}Si_{pw}$ results from the precipitation of authigenic alumino-silicates in the sediments, which preferentially incorporate the light ^{28}Si isotope (Tatzel et al., 2015; Geilert et al., 2016). Previous studies have demonstrated that formation of authigenic alumino-silicate minerals in marine sediments can either operate through dissolution of prevailing silicate minerals (such as $bSiO_2$) and subsequent co-precipitation with the released Al (Van Cappellen and Qiu, 1997; Dixit et al., 2001) and/or through adsorption onto Al- and Fe- oxyhydroxides and cations (mainly K and Mg) dissolved in the pore waters (Michalopoulos and Aller, 1995; Davis et al., 2002). These two processes likely coexist in the sediments and are herein mentioned as reverse weathering.

During reverse weathering, the dissolution of $bSiO_2$ in the sediment leads to the co-precipitation of Si and Al as a function of the availability of reactive material in the pore water (e.g. Michalopoulos and Aller, 1995; Van Cappellen and Qiu, 1997; Loucaides et al., 2011). The formation of authigenic alumino-silicate minerals through dissolution of prevailing silicate minerals and re-precipitation of pore water silicic acid has been reported for opal-rich sediments of the Southern Ocean (Van Cappellen and Qiu, 1997). It has been suggested that this process is associated with a fractionation factor between the precipitates and the pore waters estimated at −2.0‰ (Ehlert et al., 2016), where light isotopes are preferentially incorporated into the solid phase, whereas the fluid phase is enriched in ^{30}Si (Geilert et al., 2015). The evolution of the isotopic composition of both the source and product of these reactions are commonly described using two theoretical models representing a closed or open system (Fry, 2006). Using the equations defining these models we can estimate the fraction of silicic acid that need to be removed from the pore water (i.e. precipitate as authigenic alumino-silicates) to increase the predicted $\delta^{30}Si$ to match the measured $\delta^{30}Si_{pw}$ values (see supplementary material for more details on the calculation). Using this approach with either model (closed or open) gave very similar results because of the moderate to low Si incorporation compared to the pore water silicic acid reservoir (see Table S1). Because of the dynamic nature of the pore water in the sediment, the results from the open model are presented. In the SAZ, between 4% and 20% (12 ± 5% on average) of the pore water silicic acid originating from $bSiO_2$ dissolution would have been consumed to precipitate authigenic alumino-silicates and generate the observed $\delta^{30}Si_{pw}$ value. At 67°S in the AZ, between 1% and 45% (on average 17 ± 13%) of the pore water silicic acid is consumed to precipitate authigenic alumino-silicates. Higher contributions of reverse weathering in the southernmost and northernmost extremes of the transect were probably stimulated by enhanced burial of Al-bearing detrital material already observed along this transect during AESOPS (Sayles et al., 2001; Chase et al., 2003). Indeed, it has been suggested that higher Al concentration in the sediments and pore water likely favored the precipitation of authigenic aluminosilicate (Van Cappellen and Qiu, 1997).

4.3. Limitations and paleoceanographic implications

High levels of opal production in the surface ocean to the south of the PF and the impressive abundance of $bSiO_2$ in the opal belt sediments makes the Southern Ocean one of the most important Si sinks and Si burial regions in the global ocean (DeMaster, 2002; Pondaven et al., 2000; Chase et al., 2015). Diatom Si isotope records from Southern Ocean sediments have been used to evaluate silicic acid utilization across glacial cycles in Earth's recent history, often in the context of explaining glacial-interglacial variability in atmospheric pCO_2 (e.g. Brzezinski et al., 2002; Beucher et al., 2007; Dumont et al., 2020). These interpretations assume that $\delta^{30}Si_{BSi}$ records reflect past changes in nutrient use with fidelity. Our ability to evaluate the unique characteristics of past ocean C and nutrient cycling, and their variations over geological timescales depend on our ability to provide reliable records of these changes using geochemical proxies such as $\delta^{30}Si_{BSi}$. To our knowledge, only a few studies have examined how well modern sedimentary $\delta^{30}Si_{BSi}$ reflects silicic acid utilization in the surface ocean and how well this sedimentary record is preserved in the sediment (e.g. Egan et al., 2012; Pickering et al., 2020).

The ability to compare Si isotopes in both $bSiO_2$, lithogenic silica and in pore water in the present study allows us to further investigate the potential alteration of deposited $bSiO_2$ associated with early diagenesis. Using a simple mixing model between dissolving sedimentary opal and the overlying seawater and investigating the deviations of the measured $\delta^{30}Si_{pw}$ from this model allows for a semi-quantitative evaluation of the processes controlling the Si isotope dynamics within the sediment. The main limit of this approach is associated with the assumption that the $\delta^{30}Si_{BSi}$ of sedimentary opal and $\delta^{30}Si_{DSi}$ of bottom water values are constant. This assumption can be oversimplified in sediments since: (i) We expect $\delta^{30}Si_{BSi}$ to change with

time (or with sediment depth horizon) depending on the degree of silicic acid consumption in surface waters by diatoms, and on diatom species successions with different isotopic compositions during the bloom. As described in Section 4.2.1, we are confident that our approach is relatively unbiased in the SAZ and PFZ where $\delta^{30}Si_{BSi}$ is homogeneous within the core, but must be considered with caution in the AZ (see Section 4.2.1). Moreover, such approach will be unrealistic if applied on longer sediment cores where variations of $\delta^{30}Si_{BSi}$ are expected. (ii) Although a great care has been taken in this study to isolate the diatom fraction from the other siliceous particles, it is impossible to discriminate the fraction of the pore water that originates from the dissolution of other siliceous organisms such as sponges or Rhizaria. In this study, a systematic qualitative screening of the samples (before sieving) revealed only a limited amount of Rhizaria and the absence of sponge spicule in the cores. In these conditions, the preferential dissolution of diatom opal compared to the opal from these bigger organisms that dissolve much slower (Maldonado et al., 2019; Llopis Monferrer et al., 2021) suggests that the contribution of non-diatom opal to the pore water silicic acid in our study was likely to be negligible. It is however an important parameter that could limit the interpretation of the contribution of diatom dissolution to pore water $\delta^{30}Si$ variations and that need to be considered in future studies.

An additional concern that was already discussed in Section 4.2.1 is whether there is an isotopic effect associated with the dissolution of $bSiO_2$. Although this dataset does not directly test the effect of isotopic fractionation of Si isotope during $bSiO_2$ dissolution, it provides evidence leaning toward the absence of an isotope effect associated with $bSiO_2$ dissolution (see Section 4.2.1. for more details). However, it is important to keep in mind that we are considering here the absence of an "apparent" isotopic fractionation of Si isotopes, meaning that $bSiO_2$ dissolution does not measurably affect $\delta^{30}Si_{BSi}$ nor $\delta^{30}Si_{pw}$, either due to the lack of a true fractionation factor during dissolution ($^{30}\varepsilon_{Diss} = 0$) or due to the occurrence of other processes that would balance the effect of $^{30}\varepsilon_{Diss}$ such as for example the near complete loss of the frustules that undergo dissolution. Additional measurements, controlled experiments and modelling efforts are required to fully address whether the dissolution of $bSiO_2$ fractionates Si isotopes in the marine environment.

Our results show that, in the Southern Ocean, almost 90% of the silicic acid present in the pore water is associated with the dissolution of $bSiO_2$. That loss does not seem to alter the isotopic composition of the $bSiO_2$, a priori confirming its use as a reliable tool to reconstruct past variations of silicic acid utilization from diatom opal preserved in the sediments. Interestingly, the $\delta^{30}Si_{BSi}$ value of the opal raining down to the sea floor estimated from the seasonally integrated isotopic composition of opal measured in deep sediment traps differs by more than 0.5‰ compared to sedimentary $\delta^{30}Si_{BSi}$ in the AZ and SAZ (Fig. 6). Indeed, the isotopic composition of sinking diatom has been previously investigated along the same transect using particles collected from a sediment trap mooring located at 63°S in

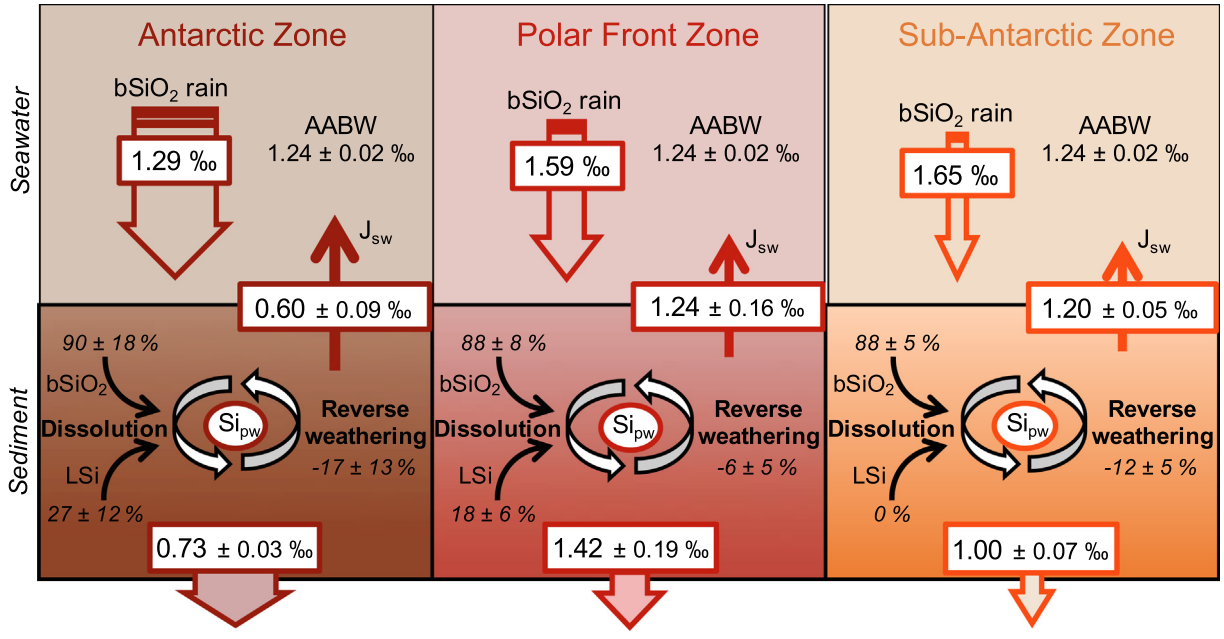

Fig. 6. Schematic view of the interactions between the different Si fluxes and $\delta^{30}Si$ values (indicated in italic) at the seawater-sediment interface for the three main zones of the Southern Ocean (J_{sw} represents the diffusive flux of dissolved Si from pore waters to the bottom ocean). $\delta^{30}Si$ of the $bSiO_2$ rain is from Closset et al., 2015; the $\delta^{30}Si_{BSi}$ and $\delta^{30}Si_{pw}$ are the averaged isotopic composition of the Si pools in the first cm of the sediment (this study). In the sediment, the % represent the fraction of pore water silicic acid that originate from the dissolution of either $bSiO_2$ or from lithogenic silica (LSi) (>0%) and that need to be consumed by reverse weathering to produce the observed $\delta^{30}Si_{pw}$ (<0%; see Section 4.3. for more details).

the AZ (Varela et al., 2004) and both in the AZ, PFZ and SAZ along a transect at 170°E (Closset et al., 2015). Although these two transects are geographically distant, the seasonal variations of the isotopic composition of sinking particles were comparable, supporting the extrapolation of measurements from Closset et al. (2015) and the use of their estimation of the seasonally integrated $\delta^{30}Si$ values for the PFZ and SAZ that are missing from Varela et al. (2004). The fact that the timescale recorded by the sediments and sediment traps differ significantly (the diatom flux was measured in 2001–2002 for the trap vs. surface sediments ranging in age from 107 and 7226 yr BP (Closset et al., 2015; Robinson et al., 2020) likely partly explain the differences in $\delta^{30}Si_{BSi}$ between traps and surface sediments. Other contributing factors may include: (i) The sediment cores from the AZ were collected south of the Southern Antarctic Circumpolar Current Front (SACCF) while the sediment traps were located north of this front in a region where diatoms would experience more Si-depleted conditions in the surface mixed layer (Fig. 1) and thus have a higher $\delta^{30}Si$ value. (ii) Higher rates of reverse weathering in the SAZ may contribute by precipitating preferentially lighter Si isotopes lowering the $\delta^{30}Si_{BSi}$ value of sedimentary diatoms. The fact that the highest mismatch (more than 0.5‰) is observed in the AZ and SAZ (Fig. 6) where reverse weathering consumes a more significant amount of pore water silicic acid (>10% of the pore water silicic acid can be re-precipitated as authigenic alumino-silicate), but is less pronounced in the PFZ, point out toward a significant alteration of the isotopic composition of sedimentary diatoms associated with the precipitation of authigenic alumino-silicate. It has been recently suggested that sedimentary diatom $bSiO_2$ is the critical substrate of authigenic alumino-silicate precipitates (Pickering et al., 2020). Clearly, further investigations of the different pool of Si co-occurring in the sediment, their respective Si isotopic composition and the complex interplay between them are necessary to fully exploit $\delta^{30}Si_{BSi}$ of sedimentary diatoms as proxy for past silicic acid utilization in the surface ocean.

5. CONCLUSION

In this study, we investigated the processes affecting the Si isotope composition of $bSiO_2$ and pore water silicic acid during early diagenesis in marine sediments of the Southern Ocean by comparing the silicic acid and $bSiO_2$ concentration data with their isotopic compositions from five sediment cores influenced by different biological production and sedimentation regimes.

Silicic acid fluxes reveal that the majority of the settling $bSiO_2$ is dissolved Southern Ocean-wide in the upper few centimeters of the sediment directly below the sediment–water interface, driving the silicic acid concentration in pore waters and the benthic flux of Si to the deep ocean. The diffusive flux of Si out of the sediments shows a clear zonal trend, with a maximum near the PF and the lowest value occurring in the SAZ. This zonal trend matches closely the spatial distribution of the sediment $bSiO_2$ content likely reflecting diatoms' productivity of the overlying water column.

Pore water silicic acid concentration and isotopic composition, combined for the first time with those of both $bSiO_2$ and lithogenic phases, helped to decipher the relative contribution of marine early diagenetic processes in the Southern Ocean sediments, which would have remained undetected by elemental concentrations alone. Along the SNOWBIRDS transect, the range of $\delta^{30}Si_{pw}$ closely matched the $\delta^{30}Si_{BSi}$ preserved in the cores suggesting that the observed increase in pore water silicic acid concentrations is primarily associated with the dissolution of $bSiO_2$. In the SAZ, the control of the $bSiO_2$ dissolution on silicic acid pore water is less significant compared to the other zones of the Southern Ocean with the upper part of the sediment influenced by both mixing with bottom water that dilute the Si concentration signal, and the deeper part of the core influenced by the precipitation of authigenic alumino-silicates, that leave the pore water enriched in heavy ^{30}Si isotope. In contrast, the PFZ sediment cores may have experienced some dissolution of isotopically light lithogenic silica (averaging -0.18 ± 0.10‰ in our study) that lower the $\delta^{30}Si_{pw}$ value expected from the strong control of $bSiO_2$ dissolution. The cores located in the AZ showed a $\delta^{30}Si_{pw}$ still mostly controlled by the dissolution of $bSiO_2$, but also influenced by a combination of both dissolution of lithogenic material and reverse weathering. However, since reaction rates cannot be quantified from observational data alone, our study only offers a semi-quantitative approach of the Si biogeochemical cycle within the sediments. To fully assess the dynamic nature of the system, a reaction-transport model such as the Biogeochemical Reaction Network Simulator (Regnier et al., 2002; Aguilera et al., 2005) will likely allow us to simultaneously estimate the different rates and timescales associated with the processes discussed in this study, and will be the object of a separate paper.

This study points out that silicic acid concentrations and $\delta^{30}Si_{pw}$ values of Southern Ocean pore waters are the result of a dynamic balance between the dissolution of $bSiO_2$, reactive lithogenic silica phases and Si re-precipitation. The processes involved differ significantly between regions and our results are consistent with the formation of authigenic alumino-silicates from the dissolving biogenic opal in the SAZ and in the AZ, likely stimulated by enhanced burial of Al-bearing detrital materials from different origin in these two regions. This observation has important implications when interpreting paleoceanographic reconstruction based on $\delta^{30}Si$ of diatoms preserved in the sediment since there are large isotopic differences between phases formed abiotically in sediments and $bSiO_2$ deposited from the overlying waters. The solubility of these authigenic silicates is poorly constrained and a recent study has shown that sedimentary diatom $bSiO_2$ is a critical substrate of early authigenic Si precipitates (Pickering et al., 2020). This implies that, even if the $\delta^{30}Si$ of diatoms preserved in the sediments is a reliable proxy for silicic acid utilization in the past ocean, if care is not taken to extract a clean $bSiO_2$ phase from sediments isotopic records could be biased.

Declaration of Competing Interest

The authors declare that they have no known competing financial interests or personal relationships that could have appeared to influence the work reported in this paper.

ACKNOWLEDGEMENTS

This work was supported by grants from the National Science Foundation (1341464 to RSR and 1341432 to MAB). The authors are especially grateful to J. Dodd and two anonymous reviewers for their constructive comments that helped us improving the manuscript. We also thank Matthew S. Fantle for his insightful editing. Authors gratefully thank the Captain and crew to the N. B. Palmer and the USAP scientific support staff on NBP1702 as well as the shipboard scientific party for their dedication and invaluable assistance in sample collection. Data will be archived in the U.S. Antarctic Program Data Center (https://www.usap-dc.org/view/project/p0010083) upon publication. The authors declare that they have no conflict of interest.

APPENDIX A. SUPPLEMENTARY MATERIAL

Supplementary data to this article can be found online at https://doi.org/10.1016/j.gca.2022.04.010.

REFERENCES

Abraham K., Opfergelt S., Fripiat F., Cavagna A.-J., de Jong J. T. M., Foley S. F., André L. and Cardinal D. (2008) δ^{30}Si and δ^{29}Si determination on USGS BHVO-1 and BHVO-2 reference materials with a new configuration on a Nu plasma multi-collector ICP-MS. *Geostand. Geoanal. Res.* **32**(2), 193–202.

Aguilera D. R., Jourabchi P., Spiteri C. and Regnier P. (2005) A knowledge-based reactive transport approach for the simulation of biogeochemical dynamics in Earth systems. *Geochem. Geophys. Geosyst.* **6**.

Beucher C. P., Brzezinski M. A. and Crosta X. (2007) Silicic acid dynamics in the glacial sub-Antarctic: Implications for the silicic acid leakage hypothesis. *Global Biogeochem. Cycles* **21**, GB2015.

Bidle K. D. and Azam F. (1999) Accelerated dissolution of diatom silica by marine bacterial assemblages. *Nature* **397**, 508–512.

Brzezinski M. A. and Nelson D. M. (1995) The annual silica cycle in the Sargasso Sea near Bermuda. *Deep-Sea Res. Part I Oceanogr.* **42**, 1215–1237.

Brzezinski M. A., Nelson D. M., Franck V. M. and Sigmon D. E. (2001) Silicon dynamics within an intense open-ocean diatom bloom in the Pacific sector of the Southern Ocean. *Deep-Sea Res. II* **48**, 3997–4018.

Brzezinski M. A., Pride C. J. and Frank V. M. (2002) A switch from $Si(OH)_4$ to NO_3^- depletion in the glacial Southern Ocean. *Geophys. Res. Lett.* **29**(12).

Brzezinski M. A. and Jones J. L. (2015) Coupling of the distribution of silicon isotopes to the meridional overturning circulation of the North Atlantic Ocean. *Deep-Sea Res. II* **116**, 79–88.

Brzezinski M. A., Closset I., Jones J. L., de Souza G. F. and Maden C. (2021) New constraints on the physical and biological controls on the silicon isotopic composition of the Arctic Ocean. *Front. Mar. Sci.* **8**, 699762.

Cardinal D., Alleman L. Y., De Jong J., Ziegler K. and André L. (2003) Isotopic composition of silicon measured by multi-collector plasma source mass spectrometry in dry plasma mode. *J. Anal. At. Spectrom.* **18**, 213–218.

Cardinal D., Alleman L. Y., Dehairs F., Savoye N., Trull T. W. and André L. (2005) Relevance of silicon isotopes to Si-nutrient utilization and Si-source assessment in Antarctic waters. *Global Biogeochem. Cycles* **19**, GB2007.

Cassarino L., Hendry K. R., Henley S. F., MacDonald E., Arndt S., Freitas F. S., Pike J. and Firing Y. L. (2020) Sedimentary nutrient supply in productive hotspots off the West Antarctic Peninsula revealed by silicon isotopes. *Global Biogeochem. Cycles* **34**.

Chase Z., Anderson R. F., Fleisher M. Q. and Kubik P. W. (2003) Accumulation of biogenic and lithogenic material in the Pacific sector of the Southern Ocean during the past 40000 years. *Deep-Sea Res. II* **50**, 799–832.

Chase Z., Kohfeld K. E. and Mustumoto K. (2015) Controls on biogenic silica burial in the Southern Ocean. *Global Biogeochem. Cycles* **29**, 1599–1616.

Closset I., Cardinal D., Bray S. G., Thil F., Djouraev I., Rigual-Hernandez A. S. and Trull T. W. (2015) Seasonal variations, origin, and fate of settling diatoms in the Southern Ocean tracked by silicon isotope records in deep sediment traps. *Global Biogeochem. Cycles* **29**, 1495–1510.

Conley D. J., Frings P. J., Fontorbe G., Clymans W., Stadmark J., Hendry K. R., Marron A. O. and De La Rocha C. L. (2017) Biosilicification drives a decline of dissolved Si in the oceans through geologic time. *Front. Mar. Sci.* **4**, 397.

Davis C. C., Chen H.-W. and Edwards M. (2002) Modeling silica sorption to iron hydroxide. *Environ. Sci. Technol.* **36**(4), 582–587.

De La Rocha C. L., Brzezinski M. A. and DeNiro M. J. (1997) Fractionation of silicon isotopes by marine diatoms during biogenic silica formation. *Geochim. Cosmochim. Acta* **61**(23), 5051–5056.

De La Rocha C. L., Brzezinski M. A., DeNiro M. J. and Shemesh A. (1998) Silicon-isotope composition of diatoms as an indicator of past oceanic change. *Nature* **395**, 680–683.

Delstanche S., Opfergelt S., Cardinal D., Elsass F., André L. and Delvaux B. (2009) Silicon isotopic fractionation during adsorption of aqueous monosilicic acid onto iron oxide. *Geochim. Cosmochim. Acta* **73**, 923–934.

Demarest M. S., Brzezinski M. A. and Beucher C. P. (2009) Fractionation of silicon isotopes during biogenic silica dissolution. *Geochim. Cosmochim. Acta* **73**, 5572–5583.

DeMaster D. (1981) The supply and accumulation of silica in the marine environment. *Geochim. Cosmochim. Acta* **45**, 1715–1732.

DeMaster D. (2002) The accumulation and cycling of biogenic silica in the Southern Ocean: Revisiting the marine silica budget. *Dee-Sea Res. II* **49**, 3155–3167.

De Salas M. F., Eriksen R., Davidson A. T. and Wright S. W. (2011) Protistan communities in the Australian sector of the Sub-Antarctic Zone during SAZ-Sense. *Deep-Sea Res. II* **58**, 2135–2149.

de Souza G. F., Reynolds B. C., Johnson G. C., Bullister J. L. and Bourdon B. (2012a) Silicon stable isotope distribution traces Southern Ocean export of Si to the eastern South Pacific thermocline. *Biogeosciences* **9**, 4199–4213.

de Souza G. F., Reynolds B. C., Rickli J., Frank M., Saito M., Gerringa L. J. A. and Bourdon B. (2012b) Southern Ocean control of silicon stable isotope distribution in the deep Atlantic Ocean. *Global Biogeochem. Cycles* **26**, GB2035.

Dixit S., Van Cappellen P. and van Bennekom A. J. (2001) Processes controlling solubility of biogenic silica and pore water build-up of silicic acid in marine sediments. *Mar. Chem.* **73**, 333–352.

Dumont M., Pichevin L., Geibert W., Crosta X., Michel E., Moreton S., Dobby K. and Ganeshram R. (2020) The nature of deep overturning and reconfigurations of the silicon cycle across the last deglaciation. *Nat. Commun.* **11**, 1534.

Egan K. E., Rickaby R. E. M., Leng M. J., Hendry K. R., Hermoso M., Sloane H. J., Bostock H. and Halliday A. N. (2012) Diatom silicon isotopes as a proxy for silicic acid utilisation: A Southern Ocean core top calibration. *Geochim. Cosmochim. Acta* **96**, 174–192.

Ehlert C., Doering K., Wallmann K., Scholz F., Sommer S., Grasse P., Geilert S. and Frank M. (2016) Stable silicon signature of marine pore waters – Biogenic opal dissolution versus authigenic clay mineral formation. *Geochem. Cosmochim. Acta* **191**, 102–117.

Frank V. M., Brzezinski M. A., Coale K. H. and Nelson D. M. (2000) Iron and silicic acid concentrations regulate Si uptake north and south of the Polar Zone in the Pacific sector of the Southern Ocean. *Deep-Sea Res. II* **47**, 3315–3338.

Frings P. (2017) Revisiting the dissolution of biogenic Si in marine sediments: A key term in the ocean Si budget. *Acta Geochim.* **36**, 429–432.

Fry B. (2006) *Stable Isotope Ecology*. Springer Science Business Media LLC, New York.

Geilert S., Vroon P. Z., Roerdink D. L., Van Cappellen P. and van Bergen M. J. (2014) Silicon isotope fractionation during abiotic silica precipitation at low temperatures: Inferences from flow-through experiments. *Geochim. Cosmochim. Acta* **142**, 95–114.

Geilert S., Vroon P. Z., Kelle N. S., Gusbrandsson S., Stefansson A. and van Bergen M. J. (2015) Silicon isotope fractionation during silica precipitation from hot-spring waters: Evidence from the Geysir geothermal field, Iceland. *Geochem. Cosmochim. Acta* **164**, 403–427.

Geilert S., Vroon P. Z. and van Bergen M. J. (2016) Effect of diagenetic phase transformation on the silicon isotope composition of opaline sinter deposits of Geysir, Iceland. *Chem. Geol.* **433**, 57–67.

Geilert S., Grasse P., Doering K., Wallmann K., Elhert C., Scholz F., Frank M., Schmidt M. and Hensen C. (2020) Impact of ambient conditions on the Si isotope fractionation in marine pore fluids during early diagenesis. *Biogeosciences* **17**, 1745–1763.

Georg R. B., Reynolds B. C., Frank M. and Halliday A. N. (2006) New sample preparation techniques for the determination of Si isotopic compositions using MC-ICPMS. *Chem. Geol.* **235**, 95–104.

Grasse P., Brzezinski M. A., Cardinal D., de Souza G. F., Andersson P., Closset I., Cao Z., Dai M., Ehlert C., Estrade N., François R., Frank M., Jiang G., Jones J. L., Kooijman E., Liu Q., Lu D., Pahnke K., Ponzevera E., Schmitt M., Sun X., Sutton J. N., Thil F., Weis D., Wetzel F., Zhang A., Zhang J. and Zhang Z. (2017) GEOTRACES inter-calibration of the stable silicon isotope composition of dissolved silicic acid in seawater. *J. Anal. At. Spectrom.* **32**, 562–578.

Grasse P., Closset I., Jones J. L., Geilert S. and Brzezinski M. (2020) Controls on Dissolved Silicon Isotopes Along the U.S. GEOTRACES Eastern Pacific Zonal Transect (GP16). *Global Biogeochem. Cycles* **34**.

Hendry K. R. H., Huvenne V. A. I., Robinson L. F., Annett A., Badger M., Jacobel A. W., Ng H. C., Opher J., Pickering R. A., Taylor M. L., Bates S. L., Cooper A., Cushman G. G., Goodwin C., Hoy S., Rowland G., Samperiz V., Ana W., Williams J. A., Achterberg E. P., Arrowsmith C., Alexander Brearley J., Henley S. F., Krause J. W., Leng M. J., Li T., McManus J. F., Meredith M. P., Perkins R. and Woodward E. M. S. (2019) The biogeochemical impact of glacial meltwater from Southwest Greenland. *Prog. Oceanogr.* **176**, 102126.

Holzer M. and Brzezinski M. A. (2015) Controls on the silicon isotope distribution in the ocean: New diagnostics from a data-constrained model. *Global Biogeochem. Cycles* **29**, 267–287.

Karl D. M. and Tien G. (1992) MAGIC: A sensitive and precise method for measuring dissolved phosphorus in aquatic environments. *Limnol. Oceanogr.* **37**(1), 105–116.

Kopczynska E. E., Dehairs F., Elskens M. and Wright S. (2001) Phytoplankton and microzooplankton variability between the Subtropical and Polar Fronts south of Australia: Thriving under regenerative and new production in late summer. *J. Geophys. Res.* **106**(C12), 31597–31609.

Llopis Monferrer N., Leynaert A., Tréguer P., Gutierrez-Rodriguez A., Moriceau B., Gallinari M., Latasa M., L'Helguen S., Maguer J. F., Safi K., Pinkerton M. H. and Not F. (2021) Role of small Rhizaria and diatoms in the pelagic silica production of the Southern Ocean. *Limnol. Oceanogr.* **66**, 2187–2202.

Loucaides S., Van Cappellen P., Roubeix V., Moriceau B. and Ragueneau O. (2011) Controls on the recycling and preservation of biogenic silica from biomineralization to burial. *Silicon*.

Maldonado M., Lopez-Acosta M., Sitja C., Garcia-Puig M., Galobart C., Ercilla G. and Leynaert A. (2019) Sponge skeletons as an important sink of silicon in the global oceans. *Nat. Geosci.* **12**, 515–822.

Meheut M., Lazzeri M., Balan E. and Mauri F. (2007) Equilibrium isotopic fractionation in the kaolinite, quartz, water system: Prediction from first-principles density-functional theory. *Geochim. Cosmochim. Acta* **71**, 3170–3181.

Michalopoulos P. and Aller R. C. (1995) Rapid clay mineral formation in Amazon Delta sediments: Reverse weathering and oceanic element cycles. *Science* **270**(5236), 614–617.

Milligan A. J., Varela D. E., Brzezinski M. A. and Morel F. M. M. (2004) Dynamics of silicon metabolism and silicon isotopic discrimination in a marine diatom as a function of pCO_2. *Limnol. Oceanogr.* **49**(2), 322–329.

Morley D. W., Leng M. L., Mackay A. W., Sloane H. J., Rioual P. and Battarbee R. W. (2004) Cleaning of lake sediment samples for diatom oxygen isotope analysis. *J. Paleolimnol.* **31**, 391–401.

Ng H. C., Cassarino L., Pickering R. A., Malcolm E., Woodward S., Hammond S. J. and Hendry K. R. (2020) Sediment efflux of silicon on the Greenland margin and implications for the marine silicon cycle. *Earth Planet. Sci. Lett.* **529**, 115877.

Orsi A. H., Whiworth, III, T. and Nowlin, Jr., W. D. (1995) On the meridional extent and fronts of the Antarctic Circumpolar Current. *Deep-Sea Res. I* **42**(5), 641–673.

Panizzo V. N., Mackay G. E. A., Mackay A. W., Vologina E., Sturm M., Pashley V. and Horstwood M. S. A. (2016) Insights into the transfer of silicon isotopes into the sediment record. *Biogeosciences* **13**, 147–157.

Paul D., Skrzypek G. and Forizs I. (2007) Normalization of measured stable isotopic compositions to isotope reference scales – A review. *Rapid Commun. Mass Spectrom.* **21**, 3006–3014.

Pickering R., Cassarino L., Hendry K. R., Wang X. L., Maiti K. and Krause J. W. (2020) Using stable isotopes to disentangle marine sedimentary signals in reactive silicon pools. *Geophys. Res. Lett.*.

Pondaven P., Ragueneau O., Tréguer P., Hauvespre A., Dezileau L. and Reyss J. L. (2000) Resolving the 'opal paradox' in the Southern Ocean. *Nature* **405**, 168–172.

Rabouille C., Gaillard J.-F., Tréguer P. and Vincendeau M.-A. (1997) biogenic silica recycling in surficial sediments across the Polar Front of the Southern Ocean (Indian Sector). *Deep-Sea Res. II* **44**(5), 1151–1176.

Regnier P., O'Kane J., Steefel C. and Vanderborght J. (2002) Modeling complex multi-component reactive-transport sys-

tems: Towards a simulation environment based on the concept of a Knowledge Base. *Appl. Math. Model.* **26**, 913–927.

Reynolds B. C., Frank M. and Halliday A. N. (2006) Silicon isotope fractionation during nutrient utilization in the North Pacific. *Earth Planet. Sci. Lett.* **244**, 431–443.

Reynolds B. C., Aggarwal J., André L., Baxter D., Beucher C., Brzezinski M. A., Engström E., Georg R. B., Land M., Leng M. J., Opfergelt S., Rodushkin I., Sloane H. J., van den Boorn S. H. J. M., Vroon P. Z. and Cardinal D. (2007) An inter-laboratory comparison of Si isotope reference materials. *J. Anal. At. Spectrom.* **22**, 561–568.

Robinson R. S., Jones C. A., Kelly R. P., Love A., Closset I., Rafter P. A. and Brzezinski M. (2020) A test of the diatom-bound paleoproxy: Tracing the isotopic composition of nutrient-nitrogen into Southern Ocean particles and sediments. *Global Biogeochem. Cycles* **34**.

Roerdink D. L., van den Boom S. H. J. M., Geilert S., Vroon P. Z. and van Bergen M. J. (2015) Experimental constraints on kinetic and equilibrium silicon isotope fractionation during the formation of non-biogenic chert deposits. *Chem. Geol.* **402**, 41–51.

Savage P. S., Georg R. B., Williams H. M. and Halliday A. N. (2013) The silicon isotope composition of the upper continental crust. *Geochim. Cosmochim. Acta* **109**, 384–399.

Sayles F. L., Martin W. R., Chase Z. and Anderson R. F. (2001) Benthic remineralization and burial of biogenic SiO_2, $CaCo_3$, organic carbon, and detrital material in the Southern Ocean along a transect at 170° West. *Deep-Sea Res. II* **48**, 4323–4383.

Schulz H. D. (2006) Quantification of early diagenesis: Dissolved constituents in pore water and signals in the solid phase. In *Marine Geochemistry* (eds. H. D. Schulz and M. Zabel). Springer, Berlin, Heidelberg.

Sun X., Olofsson M., Andersson P. S., Fry B., Legrand C., Humborg C. and Morth C.-M. (2014) Effects of growth and dissolution on the fractionation of silicon isotopes by estuarine diatoms. *Geochim. Cosmochim. Acta* **130**, 156–166.

Sutton J. N., Varela D. E., Brzezinski M. A. and Beucher C. P. (2013) Species-dependent silicon isotope fractionation by marine diatoms. *Geochim. Cosmochim. Acta* **104**, 300–309.

Sutton J. N., André L., Cardinal D., Conley D. J., de Souza G. F., Dean J., Dodd J., Elhert C., Ellwood M. J., Frings P. J., Grasse P., Hendry K., Leng M. J., Michalopoulos P., Panizzo V. N. and Swann G. E. A. (2018) A review of the stable isotope bio-geochemistry of the global silicon cycle and its associated trace elements. *Front. Earth Sci.* **5**, 112.

Tatzel M., von Blanckenburg F., Oelze M., Schuessler J. A. and Bohrmann G. (2015) The silicon isotope record of early silica diagenesis. *Earth Planet. Sci. Lett.* **428**, 293–303.

Tréguer P. J. and De La Rocha C. L. (2013) The world ocean silica cycle. *Annual Rev. Marine Sci.* **5**, 477–501.

Tréguer P. J. (2014) The Southern Ocean silica cycle. *C.R. Geosci.* **346**, 279–286.

Tréguer P. J., Sutton J. N., Brzezinski M. A., Charette M. A., Devries T., Dutkiewicz S., Ehlert C., Hawkings J., Leyneart A., Liu S. M., Llopis M. N., Lopez-Acosta M., Maldonado M., Rahman S., Rau L. and Rouxel O. (2021) Reviews and syntheses: The biogeochemical cycle of silicon in the modern ocean. *Biogeosciences* **18**, 1269–1289.

Trull T., Rintoul S. R., Hadfield M. and Abraham E. R. (2001) Circulation and seasonal evolution of polar waters south of Australia: Implications for iron fertilization of the Southern Ocean. *Deep-Sea Res. II* **48**, 2439–2466.

Van Cappellen P. and Qiu L. (1997) Biogenic silica dissolution in sediment of the Southern Ocean. I. Solubility. *Deep-Sea Res. II* **44**(5), 1109–1128.

Van Cappellen P., Dixit S. and van Beusekom J. (2002) Biogenic silica dissolution in the oceans: Reconciling experimental and field-based dissolution rates. *Global Biogeochem. Cycles* **16**(4), 1075.

Varela D. E., Pride C. J. and Brzezinski M. A. (2004) Biological fractionation of silicon isotopes in Southern Ocean surface waters. *Global Biogeochem. Cycles* **18**, GB1047.

Wetzel F., de Souza G. F. and Reynolds B. C. (2014) What controls silicon isotope fractionation during dissolution of diatom opal?. *Geochim. Cosmochim. Acta* **131**, 128–137.

Ziegler K., Chadwick O. A., Brzezinski M. A. and Kelly E. F. (2005) Natural variations of d30Si ratios during progressive basalt weathering, Hawaiian Islands. *Geochim. Cosmochim. Acta* **69**(19), 4597–4610.

Associate editor: Matthew S. Fantle